TU Delft

Delft University of Technology

Document Version
Final published version

Licence
CC BY

Citation (APA)
Geerts, D., Liu, W., Daniilidis, A., & Kramer, G. J. (2026). Sizing optimization of district heating components with High-Temperature Aquifer Thermal Energy Storage: Techno-economic analysis for different renewable energy levels. *Energy*, *353*, Article 140931. https://doi.org/10.1016/j.energy.2026.140931

Important note
To cite this publication, please use the final published version (if applicable).
Please check the document version above.

Copyright
In case the licence states “Dutch Copyright Act (Article 25fa)”, this publication was made available Green Open Access via the TU Delft Institutional Repository pursuant to Dutch Copyright Act (Article 25fa, the Taverne amendment). This provision does not affect copyright ownership.
Unless copyright is transferred by contract or statute, it remains with the copyright holder.

Sharing and reuse
Other than for strictly personal use, it is not permitted to download, forward or distribute the text or part of it, without the consent of the author(s) and/or copyright holder(s), unless the work is under an open content license such as Creative Commons.

Takedown policy
Please contact us and provide details if you believe this document breaches copyrights.
We will remove access to the work immediately and investigate your claim.

This work is downloaded from Delft University of Technology.

Energy 353 (2026) 140931

Contents lists available at ScienceDirect

Energy

journal homepage: www.elsevier.com/locate/energy

Sizing optimization of district heating components with High-Temperature Aquifer Thermal Energy Storage: Techno-economic analysis for different renewable energy levels

David Geerts [a,c,*], Wen Liu [a], Alexandros Daniilidis [b], Gert Jan Kramer [a]

[a] Copernicus Institute of Sustainable Development, Heidelberglaan 8, 3584 CS, Utrecht, The Netherlands
[b] Faculty of Civil Engineering and Geosciences, Stevinweg 1, 2628 CN, Delft, The Netherlands
[c] IF Technology, Velperweg 35, 6824 BE, Arnhem, The Netherlands

ARTICLE INFO

Keywords:
High-Temperature Aquifer Thermal Energy Storage
District heating
Levelized cost of heat
Sizing optimization
Geothermal heat
Solar thermal collector

ABSTRACT

District heating systems must decarbonize by replacing fossil fuel-based heat sources with sustainable alternatives. To fully utilize the capacity of renewable sources, seasonal thermal energy storage is necessary due to seasonal supply–demand mismatches. High-Temperature Aquifer Thermal Energy Storage (HT-ATES) offers a promising solution, but its cost-effective deployment requires coordinated sizing with the sustainable heat source, which has received limited attention in literature. This study presents a techno-economic and renewable share analysis of district heating systems incorporating deep geothermal heat, solar thermal collectors, HT-ATES, and gas boilers. We identified representative heat demand profiles for different climates by clustering to ensure broader applicability of the findings. We show that the demand profile is important for the cost-effectiveness of district heating. The results show that HT-ATES is cost-effective in most scenarios compared to natural gas boilers, particularly when paired with a geothermal source. Geothermal energy was generally more economically favorable than solar thermal collectors. Achieving 100% renewable heat supply is cost-inefficient because it requires large additional capacity for limited additional load, increasing costs by 15% compared to 99% renewable share. However, 90% renewable share can be reached with only 5% cost increase compared to the optimum, using geothermal energy. These insights provide guidance for district heating designers, operators and policymakers on optimal component sizing and promote the informed use of HT-ATES to support cost-effective decarbonization of district heating. Representative demand profiles are expected to be used often in research, as they proved influential on the levelized cost of heat.

1. Introduction

Reducing greenhouse gas emissions is crucial, and heating and cooling accounts for approximately 65% of global building energy use [1], mostly generated by fossil fuels [2]. Additionally, the majority of people are expected to live in cities by 2050 [3], for which District Heating (DH) systems are particularly suitable. The current DH systems are mainly driven by fossil fuels and need to be transitioned to renewable sources [1,4].

Various renewable heat sources exist, such as waste incineration, solar thermal, and geothermal [5]. However, the heat supply of these technologies often mismatches with the heat demand. For example, solar heat is seasonal in colder climates, while waste incineration heat and geothermal heat preferably operate year-round. Heat demand also varies seasonally and geographically, leading to a seasonal mismatch between heat supply and demand.

Thermal Energy Storage (TES) can address this seasonal mismatch, but to do so for a DH system, the storage technology must be both large-scale and cost-effective. Underground Seasonal Thermal Energy Storage (USTES) technologies are suitable due to their small surface area requirement; examples include Borehole Thermal Energy Storage (BTES), and Cavern Thermal Energy Storage (CTES), with Yang et al. [6] providing an overview of relevant projects. This study focuses on High-Temperature Aquifer Thermal Energy Storage (HT-ATES), which stores heat in an aquifer [7,8].

Most Aquifer Thermal Energy Storage (ATES) systems function at temperatures below 25 °C, often used for individual buildings [7].

* Corresponding author at: Copernicus Institute of Sustainable Development, Heidelberglaan 8, 3584 CS, Utrecht, The Netherlands.
E-mail address: d.c.geerts@uu.nl (D. Geerts).

https://doi.org/10.1016/j.energy.2026.140931
Received 10 October 2025; Received in revised form 12 March 2026; Accepted 31 March 2026
Available online 6 April 2026
0360-5442/© 2026 The Authors. Published by Elsevier Ltd. This is an open access article under the CC BY license (http://creativecommons.org/licenses/by/4.0/).

Abbreviations

BTES	Borehole Thermal Energy Storage
CapEx	Capital Expenditure
CF	Cost Factor
CF-A	Cost Factor HT-ATES
CF-G	Cost Factor Geothermal
CF-S	Cost Factor STC
CTES	Cave Thermal Energy Storage
DH	District Heating
ES	Energy Share
GAG	Geothermal + HT-ATES + gas boiler
HT-ATES	High-Temperature Aquifer Thermal Energy Storage
LCOH	Levelized Cost Of Heat
OpEx	Operational Expenditure
PTES	Pit Thermal Energy Storage
RES	Renewable Energy Share
SAG	STC + HT-ATES + gas boiler
STC	Solar Thermal Collector
STES	Seasonal Thermal Energy Storage
TES	Thermal Energy Storage
USTES	Underground Seasonal Thermal Energy Storage

However, this temperature is insufficient for the requirements for DH systems that need higher operational temperatures. HT-ATES, which operate above 25 °C, can be a more effective alternative to low-temperature ATES, as it can potentially supply heat directly to the DH.

In scientific literature, studies focusing on optimizing the sizing of both the renewable heat source and HT-ATES are scarce. This presents a significant knowledge gap on how the sizing of HT-ATES and renewable heat sources influences the economics of a DH system. To efficiently utilize both the renewable heat source and HT-ATES, their sizing must be coordinated and ideally optimized together, as improper sizing can be economically detrimental [9]. Several studies optimize DH heat source sizing, focusing on technologies such as CHP [10,11], heat pumps [12], Solar Thermal Collector (STC) [13,14], and biomass [15], but these studies do not include Seasonal Thermal Energy Storage (STES). Some studies do include STES, where BTES has been combined a CHP and STC [16–19], while Pit Thermal Energy Storage (PTES) was also combined with STC and CHP [20,21]. However, optimization studies for DH systems with HT-ATES are limited. Multiple studies focus solely on the HT-ATES, predicting its efficiency [22–24], analyzing maximum capacity [25] or optimizing well location [26,27]. Only a few studies consider HT-ATES in DH systems [28–30], but do not focus on the sizing of the systems.

The effect of the demand profile on the sizing of the system represents another significant knowledge gap. To the author's knowledge, none of the previous studies consider the impact of demand profiles on sizing optimization in a DH system. Heat demand has been shown to significantly differ per location [31], varying both in length of heating season and peak of heat demand compared to average demand. Since heat demand varies by location, optimal solutions differ per location and demand profile.

Based on the discussion above, the existing studies focus on the optimization of HT-ATES with limited investigation from the heating system perspective. There is a need to understand the dynamic between the size of renewable heat supply and HT-ATES and the DH system performance under different heat demand profiles. The novelty of this study lies in the simultaneous optimization of HT-ATES and renewable-source sizing across varying demand profiles. To fulfill the research objective, the following research steps are taken: (1) applying three distinctly yearly heat demand curves, derived from 55 unique geographical locations, to represent different head demand profiles; (2) analyzing the effect that component sizing and demand profile have on the economic and emission-related performance of a DH system. For DH systems with renewable heat sources and HT-ATES, the optimal component sizing is determined to minimize Levelized Cost Of Heat (LCOH), and the effect of increasing the Renewable Energy Share (RES) is explored;

2. Method overview

A DH system with the following components was evaluated: a deep geothermal doublet (referred to as geothermal), a STC, a HT-ATES, and a gas boiler. The DH LCOH was optimized by optimizing the size of the individual components for different levels of RES, and further analysis was done on the optimal points. This is separated into the following steps, which are explained in detail in the following subchapters:

1. Heat demand identification: The heat demand profile for 55 different locations was obtained; 3 distinctly different heat demands were derived through clustering for which the optimal size of DH components was calculated.
2. DH modeling: The DH was modeled, and RES and LCOH were calculated to assess the economic and emission-related impact.
3. Sizing optimization: The sizing of the different components of the DH systems was optimized with regard to the LCOH and RES.
4. Detailed optimum case analysis: A selection of optimum cases was compared to demonstrate the difference in economic (LCOH) and environmental performance (RES) of these optima.

2.1. Heat demand identification

The first step in the analysis was to obtain distinct yet representative heat demand profiles. This approach ensures that the study's findings are broadly applicable to different types and patterns of heat demand. To achieve this, heat demand data from 55 different locations were collected and subsequently clustered to identify representative demand profiles. These demand profiles can be found on GitHub [32].

The heat demand data for 55 locations were generated by using the method created by Staffel et al. [31]. This was done by using the renewable ninjas website and using the given parameters for heat demand generation. The heat demand profile was scaled to be 50 GWh in total to allow a fair comparison. The 55 locations are listed in Appendix A. These locations are geographically distributed across the northern hemisphere, excluding locations without heat demand, commonly found around the equator [31]. The locations represent major cities of each of the considered continents and were chosen to represent a wide variety of climates and corresponding heat demand patterns. The distributions of locations are shown in Fig. 1.

To enable comparability, all heat demand profiles were normalized such that their maximum value was set to one, and all other values in the temperature profile were scaled accordingly. This normalization allowed comparison between heat demands, focusing on dynamic seasonal behavior, removing the component of demand magnitude, which is dependent on the number of households connected to a DH system, differing per DH system.

The heat demand profiles were then clustered into three distinct clusters. This was done by selecting three cluster centers that minimized the total distance between each heat demand profile and its closest cluster center. Three clusters were chosen because introducing a fourth resulted in a small, insignificant cluster with too few representative (less than 3) locations to justify its inclusion. The cluster centers were used in the following steps and represent three significantly different demand profiles. Clustering was performed using the TimeSeriesKMeans function from the tslearn package in Python [33].

Fig. 1. The heat demand locations used in this study.

2.2. DH system modeling

The modeling of the DH system is explained in detail in the supplementary information and is based on Geerts et al. [9] and is available on GitHub [32]. The model includes four components: deep geothermal doublet (referred to as geothermal), STC, HT-ATES, and a natural gas boiler. The district heating systems infrastructure connecting these components is case-specific and, beyond the scope of this work, therefore, not considered.

The design of the DH system is determined by three key inputs:

1. The size of geothermal: Defined by the outgoing flow rate of the geothermal well and converted to watts using

$$E = mc\Delta T \tag{1}$$

E is the heat delivered (Watt), m is the mass flow rate (kg/s), c is the specific heat capacity (J/(kg°C)), and the used fluid is assumed to be water. ΔT represents the temperature difference (°C) between the geothermal output temperature and the return (cut-off) temperature, i.e., the temperature of the water re-injected in the geothermal well.
2. The size of the STC: Determined by total STC area, which increases the heat output of this component. The productivity of this component is dependent on the location used (see Supplementary material).
3. The size of the HT-ATES: Defined by its maximum flow rate, convertible to Watts using Eq. (1). As the output temperature of the HT-ATES declines during extraction [34], the peak thermal output (MWp) is used, which is calculated based on the temperature of the stored heat (which is the maximum temperature that can be extracted from the HT-ATES) and the cut-off temperature from the demand side.

Based on these component sizes, the gas boiler capacity is calculated to cover any remaining peak demand. Additional details on the components and the modeling approach can be found in the supplementary material.

2.3. Assessment

2.3.1. Economic assessment

The economic metric used is LCOH [35] of the system and individual components. The LCOH of individual components is used to compare the components with each other, while the system LCOH is used to compare different heating systems' costs. The demarcation for the different LCOH is shown in Fig. 2. The LCOH is defined as

$$LCOH = \frac{\sum_{t=1}^{n} \frac{I_t + O\&M_t}{(1+r)^t}}{\sum_{t=1}^{n} \frac{E_t}{(1+r)^t}}. \tag{2}$$

where I_t is the investment to install the component, r is the discount rate, n is the lifetime in years, therefore t also uses intervals of years. $O\&M$ is the cost of operation and maintenance, and E_t is the heat delivered to the demand. The lifetime of the system is chosen based on the least common multiple principle that ensures no residual value at the end of the system's life and components are replaced as needed [9]. The costs for installing and operating a DH network are not included in this analysis, as our study has the focus on the optimization of sizing, and any costs related to the pipes, pumps, and heat distribution equally affect all options that we consider and do not affect optimal sizing. Furthermore, these costs are highly location-specific and are rarely generalizable. Therefore, these costs are outside of scope. They are further discussed in Section 4. The economic and environmental parameter values for these components are provided in Table 1. There is also a price for CO_2 emissions in line with the European Emission Trading Scheme, namely 75 €/tonne CO_2 [36].

2.3.2. RES assessment

The used metric is the RES, representing the share of renewable energy that is supplied by each renewable heat source relative to the total energy delivered and calculated as

$$RES = E_{HS}/E_{tot}, \tag{3}$$

where E_{HS} is the energy delivered by the sustainable heat sources and E_{tot} is the total energy delivered to the demand. This is calculated for each component for its entire lifetime. The Energy Share (ES) refers to the energy supplied by each source. In this research, the STC, geothermal, and HT-ATES are considered to be renewable.

2.4. Calculating optimum

The optimal size of the components is calculated for the three identified demands (see Section 2.1). These demand cluster centers are scaled to represent 50 GWh of annual heat demand, to represent actual heat demand compared to the previously normalized and dimensionless demand. Two supply configurations are developed to meet the heat demand of three demand profiles:

1. Geothermal + HT-ATES + gas boiler (called GAG)
2. STC + HT-ATES + gas boiler (called SAG)

For each supply configuration and heat demand profile combination, the component sizes that result in the lowest system LCOH are identified. Each component is sized accordingly and can be minimized all the way to zero capacity, effectively being removed from the configuration. The optimal sizing of components is calculated by simulating the entire available sizing space and selecting the minimum.

Additionally, the impact of heat source performance on the LCOH and of the system is considered, as the heat source productivity may vary by location. This is accounted for using the Cost Factor (CF), which captures the costs of the heat source compared to the base costs shown in Table 1, where costs refer to both CapEx and OpEx. CF shows the impact of increasing/decreasing costs for the same productivity or

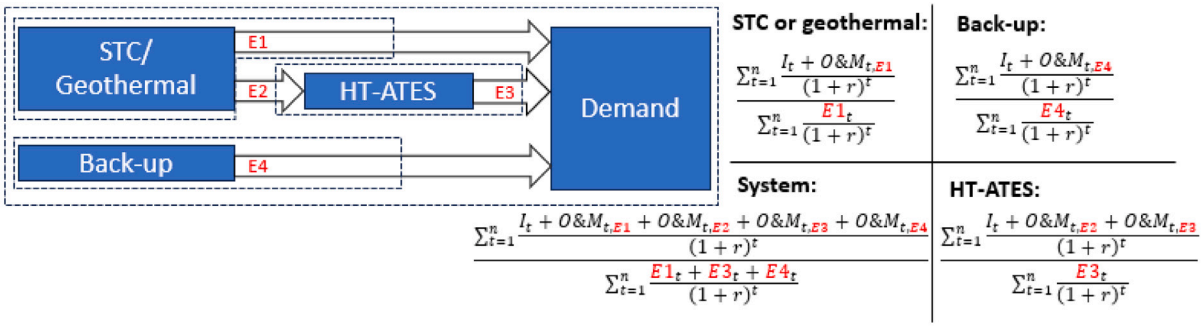

Fig. 2. The demarcation of the different LCOH calculations in this study, shown by the dotted boxes. The arrows represent energy flows between components. Note that the heat that is delivered from the sustainable source to the HT-ATES is not included in the E_t of the sustainable source. Additional costs incurred for producing this stored energy are included in the $O\&M$ costs of the HT-ATES and removed from the $O\&M$ of the sustainable source.
Source: Adapted from [6].

Table 1
Economic and environmental parameters when CF is equal to 1.

Component	Parameter	Value	Unit	Source
Geothermal	CapEx	1.9	M€/MW	[37]
	Fixed OpEx	69	k€/MW/year	[37]
	Variable OpEx	7.2	€/MWh/year	[37]
	Lifetime	30	years	[37]
	CO_2 emissions	12.5	$kgCO_2$/MWh	[38]
Gas boiler	CapEx	0.10	M€/MW	[39]
	Fixed OpEx	2.0	k€/MW/year	[39]
	Gas price (including tax)	55	€/MWh	[40]
	Lifetime	15	years	[41]
	CO_2 emissions	200	$kgCO_2$/MWh	[42]
HT-ATES	CapEx	0.010	M€/(m^3/hour injection capacity)	[29]
	Fixed OpEx	0.77	k€/(m^3/hour injection capacity)/year	[29]
	Electricity use	1.39	kWh/m^3 injected	[29]
	Electricity price	200	€/MWh	[43]
	Lifetime	30	years	[39,44]
	CO_2 emissions electricity	200	$kgCO_2$/MWh	[45]
Solar	Capex	0.43	k€/MWp	[37]
	Fixed opex	4.1	€/MWp/year	[37]
	Variable OpEx	1.9	€/MWh/year	[37]
	Lifetime	20	years	[37]
	CO_2 emissions	0	$kgCO_2$/MWh	

decreasing/increasing productivity for the same costs. Which is done to account for more, or less efficient heat sources:

$$CF = \frac{C_{source}}{C_{source,base}} \tag{4}$$

C_{source} refers to the cost parameters of a component. The subscript *base* refers to the base case parameters shown in Table 1. CF > 1 means that for the same costs, the heat source produces less heat, which can also be rephrased to higher costs for the same heat production compared to the base case. When CF is < 1, then for the same costs, the heat source produces more heat. There is further flexibility for CF, where any changes in the costs of competing technology can be reflected in an equal change in CF value. This shows the flexibility of the CF.

The CF is further divided into the Cost Factor STC (CF-S) and Cost Factor Geothermal (CF-G). This captures the effect that the source might be more or less efficient depending on location, but also includes potential future cost changes and is incorporated by changing the OpEx and CapEx values of the corresponding technology shown in Table 1.

For STC, the economic numbers are based on an STC that receives an average yearly solar irradiation of 1000 kWh/m^2. For the considered locations, the yearly solar irradiation varies between 500 and 2000 kWh/m^2. Therefore, the CF-S is given a range of 0.5 to 2 [46].

For geothermal, the CF-G the economic numbers are based on a country that has an average geothermal gradient of 30 °C/km. However, geothermal gradients globally range between 15 °C/km and 90 °C/km, excluding anomalies such as volcanic regions; these will be discussed in Section 4. Therefore, the range for CF-G is set to 0.33 and 2.

These CF-S and CF-G are combined with the previously described system configurations and demand profiles. For the STC, the CF-S values of 0.5, 1, and 2 are combined with the three demands, resulting in 9 cases. For the geothermal, the CF-G values of 0.33, 0.5, 1, and 2 are combined with the three demand profiles, resulting in 12 cases and leading to a total of 21 cases. For all 21 cases, the sizing with the lowest LCOH is calculated, and the effect of higher RES on the LCOH is analyzed.

2.5. Sensitivity analysis HT-ATES

A sensitivity analysis was conducted to evaluate the economic performance of the HT-ATES. The CF is used again (Eq. (4)) and when applied to HT-ATES, is called Cost Factor HT-ATES (CF-A). Unlike the CF-S and CF-G, which apply to heat-producing systems, the HT-ATES does not generate heat. Instead, the CF-A reflects the costs paid per unit of energy stored. HT-ATES depths typically range from 100–500 meters [38,47]. Increasing depth increases both the CapEx of the wells (linearly [28]) and the operational cost of pumping. To capture this variability in depth, the CF-A is varied between 0.5 and 2. This sensitivity analysis is conducted for a single demand to maintain conciseness, and the cluster that represents the most locations will be chosen for this sensitivity analysis.

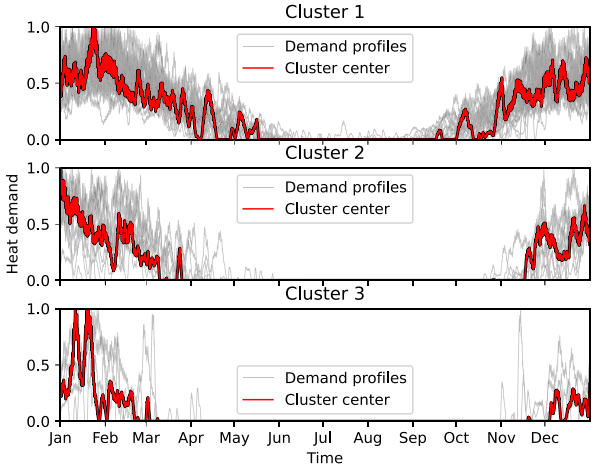

Fig. 3. The three heat profile clusters. The red line indicates the cluster center. The average demand value is 0.23, 0.13, and 0.08 for clusters 1, 2, and 3, respectively, compared to a peak of 1 for all clusters.

2.6. Detailed optimum case analysis

Building on the results from the previous subsection, key configurations are selected for further analysis. These configurations are chosen based on two criteria: (1) the sizing with the lowest system LCOH and (2) the sizing with the lowest LCOH, where the sustainable heat source and HT-ATES contribute 99% of the ES. The 99% threshold is chosen to allow other methods to be used for the last 1%, which is further discussed in Section 4. 99% is chosen as the last 1% of RES is shown to be very cost ineffective in Section 3. Additionally, to compare heat demand profiles, the optimal sizing for 99% RES will be analyzed and compared for each demand profile. The selected configurations are identified in the results section and analyzed further in terms of cost distribution and energy share. This analysis provides insights into the economic and operational performance of the most promising system configurations.

3. Results

3.1. Heat demand clustering

The heat demand in the selected locations was clustered into three clusters (Fig. 3, see Appendix A for a detailed breakdown of clusters). The clusters differ mainly in heating season length and peak-to-average demand ratio. cluster 1 has a long heating season (6 months) with moderate peaks (only 4 times higher than the average demand), cluster 2 has a shorter heating season with higher peaks compared to cluster 1, and cluster 3 has a very short heating season with very large demand peaks. Cluster 1 includes 33 data points, more than clusters 2 and 3, which have 13 and 10 data points, respectively. The cluster centers are Berlin, Chongqing, and Barcelona for clusters 1, 2, and 3, respectively.

As seen in Fig. 4, cluster 1 includes locations with colder climates (annual average temperature of all locations of ~8 °C) with longer heating seasons, while clusters 2 and 3 represent progressively warmer climates, averaging 14 °C and 20 °C of annual average temperature, respectively. The most notable outliers in the clustering results are the two locations in Japan (Osaka and Tokyo), which, despite having nearly identical average temperatures and similar geographic locations, are assigned to different clusters; both points have a large distance to their own cluster center. These outliers are further discussed in Section 3.3 to assess the robustness of the clustering.

Lastly, the average temperature map is based on data from 1951–1980, the most recent detailed open-source dataset found by the authors. While temperature values have shifted due to climate change [48], the map primarily serves to illustrate relative temperature differences between locations, which remain generally valid [48].

3.2. Sizing optimization results

In Fig. 5, the demand profiles used are shown, for which the optimal size is calculated. Most notable is that C3:Barcelona has a very high demand for a short period. The peak heat demand of the other two clusters is significantly lower, in line with observations of the previous subsection. The name of the demands is based on the cluster number and the location used.

The optimization results for GAG (geothermal + HT-ATES + gas boiler) and SAG (STC + HT-ATES + gas boiler) configurations are presented in Figs. 6 and 7, respectively.

3.2.1. Optimization results for GAG configuration

For CF-G=1, C1:Berlin and C2:Chongqing, the optimal point includes geothermal and HT-ATES (Fig. 6). In C3:Barcelona, the lowest LCOH is achieved when only gas boilers are used, as the optimal point is located at zero geothermal and HT-ATES capacity. This suggests that the lower peaks in heat demand in C1:Berlin and C2:Chongqing favor the use of geothermal and HT-ATES. The LCOH optimum for C1:Berlin and C2:Chongqing results in a RES value of 89% and 51%, respectively. Conversely, the LCOH optimum for C3:Barcelona has a RES value of 0%. Furthermore, C1:Berlin generally has the lowest LCOH values of the clusters, followed by C2:Chongqing and lastly C3:Barcelona as the highest LCOH values. Indicating that the relatively large peaks compared to average demand are expensive to cover, where the LCOH of the optimum for CF-G is 1, increases from 59 to 79 to 93 €/MWh for clusters 1, 2, and 3, respectively.

The red dots indicate that achieving RES values above 90% is highly cost-effective with HT-ATES for all clusters at CF-G=1 (Fig. 6). The final 10% of RES can be most efficiently attained by expanding HT-ATES capacity, which is more economically efficient than increasing geothermal capacity.

The red dots in C2:Chongqing, CF-G=0.5, exhibit a discontinuous behavior in the optimal sizing for minimizing LCOH with increasing RES targets. For reaching a RES value very close to 1, the cost-optimal way is by using the HT-ATES instead of increasing the geothermal capacity. For anything below 99% RES, only using geothermal is the optimal cost strategy. The optimal sizing with increasing RES "jumps" from using only geothermal with a very high capacity to a relatively small geothermal capacity with an HT-ATES, indicating that HT-ATES is economically efficient in reaching the last percentage of RES, as geothermal capacity is expensive for a lower load. In practice, this leads to a lock-in effect where the decision needs to be made early on whether to only use geothermal or use both technologies, since the cost-optimal size is very different.

Additionally, reaching 100% RES is very expensive. For CF-G = 1 in C1:Berlin, the LCOH increases from 59, 60, 65, 74 €/MWh for the RES targets of 90%, 95%, 99%, and 100%, respectively. The last one percent RES is expensive, due to requiring a large capacity for very little additional load. The peak boiler has a very low CapEx per MW of nominal capacity, roughly ten times smaller than geothermal. This means installing capacity with a low load factor is more cost-efficient with a gas boiler than with HT-ATES or geothermal. On the other hand, 90% RES could be reached with a maximum increase of LCOH of 5% compared to the optimum LCOH, for all CF-G values of 1 or lower.

Looking at the different CF-G values for C1:Berlin shows that lower CF-G values (CF-G = 0.5 or 0.33) significantly improve geothermal cost-effectiveness. The sizing with the lowest LCOH moves to a point where there is no HT-ATES capacity required, compared to when CF-G is 1. For those lower CF-G values, achieving higher RES values can be done in the most cost-efficient way by adding more geothermal capacity, due to the more cost-competitive geothermal. The same effect can also be seen for the other two clusters. For the CF-G value of 2, the gas boilers are the most cost-efficient. Additionally, for this higher CF-G value, the higher RES values are most optimally reached by a balance of HT-ATES and geothermal.

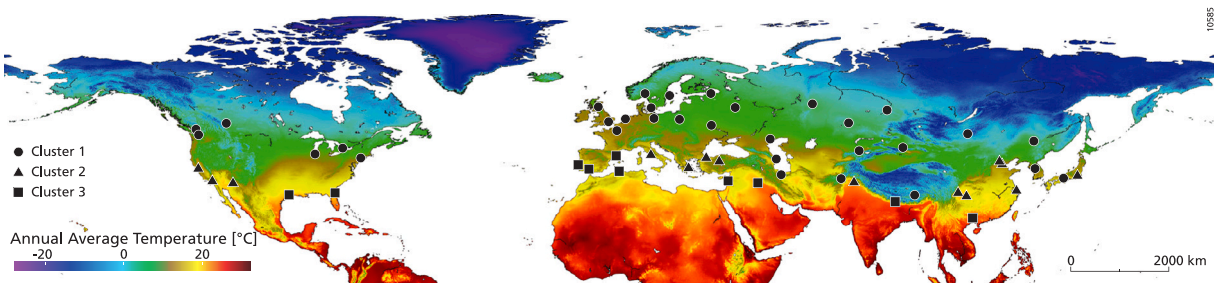

Fig. 4. The heat demand locations in the clusters. These are overlain on an annual average temperature map obtained from [49].

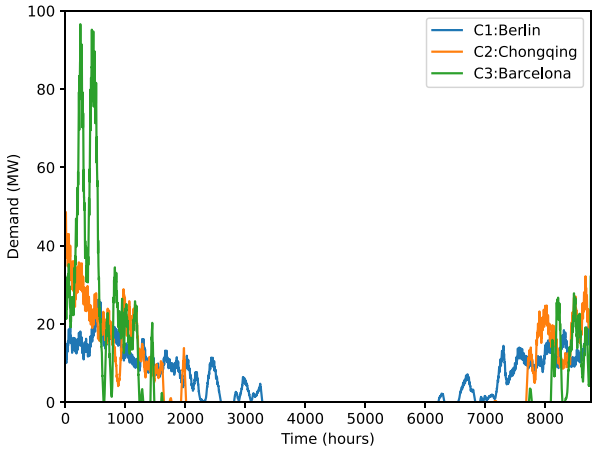

Fig. 5. The heat demand profiles used for the optimization. They are scaled to reach a total annual demand of 50 GWh.

3.2.2. Optimization results for SAG configuration

For the SAG configuration (Fig. 7), the difference between clusters is clearest at CF-S = 0.5. The lowest LCOH of both cluster 1 and 2 is a combination of both STC and HT-ATES and has a RES of 71% and 48% for cluster 1 and 2, respectively. In contrast, for C3:Barcelona, the minimum LCOH is achieved using only a gas boiler. RES values above 90% are most cost-effectively achieved by significantly increasing the HT-ATES capacity. For RES improvements below 90%, the most efficient approach is to increase both HT-ATES and STC in roughly equal proportions. The RES lines indicate that achieving values above 50% using only STC requires extremely large collector areas, leading to high LCOH values. For C3:Barcelona, reaching RES levels above 90% requires very large capacities of both STC and HT-ATES due to the mismatch between solar heat supply and heat demand. Solar thermal collectors primarily produce heat during summer, whereas demand peaks in winter, making large-scale HT-ATES essential. Also for SAG, similar to GAG, reaching 100% RES significantly increases the LCOH. For CF-S = 0.5 in C1:Berlin, the LCOH increases from 78, 80, 85, 94 €/MWh for the RES targets of 90%, 95%, 99%, and 100%, respectively.

Solar heating at CF-S = 1 is already quite expensive and not an economically competitive way to increase RES. The difference between the different CF-S values is mainly in the use of solar energy and the total system costs. Higher CF-S figures result in very high LCOH values. The red dots for C1:Berlin do not change position between CF-S = 1 and CF-S = 2, indicating the cost-optimal pathway to increase RES remains unchanged even if the cost efficiency of CF-S is reduced from CF-S = 1 to CF-S = 2. The same is observed for C2:Chongqing and C3:Barcelona, indicating that the cost-optimal pathway to increasing RES is independent of higher STC costs.

3.2.3. Comparison of GAG and SAG configurations

The difference between the optimal points for GAG and SAG configuration has three aspects. Firstly, the HT-ATES size for reaching higher RES values, where the SAG configuration requires very large HT-ATES due to the mismatch between STC supply and heat demand, where for GAG, this mismatch is less prevalent and HT-ATES is not used with all CF-G values. Secondly, when CF-S and CF-G = 1, the geothermal is much more cost-efficient than the STC, indicated by a lower LCOH at the optimum points. Lastly, a RES value of 100% is very hard to reach using only STC, whereas with CF-G values of 0.5 and 0.33, using only geothermal is the most cost-efficient method to reach RES values of 100%. For both configurations, reaching 100% RES leads to a significantly high LCOH compared to lower targets, such as 95% or 99% RES (when comparing 100% RES with 99% RES, the LCOH increased on average by 15%).

3.3. Robustness clustering

To assess the robustness of the clustering, the sizing results were evaluated for additional locations within each cluster. While several points were examined, this discussion focuses on Osaka and Tokyo, which were discussed earlier as outliers in their own cluster. The LCOH value of their optimal point is within 5% of each other, yet these values were positioned between the optimal LCOH values of their respective cluster centers. Where the two cluster centers differed by approximately 20% in terms of LCOH. This suggests that the cluster centers may not fully represent the economic performance of all points within the cluster, as the clustering was done to obtain significantly different demands. Future work could focus on more demands to find the leading cause of the differences between demand profiles.

3.4. Sensitivity results CF-A

For the sensitivity analysis, we focus on C1:Berlin as it is the largest cluster. The effect of the CF-A is shown in Figs. 8 and 9. The figures for C2:Chongqing and C3:Barcelona are shown in the supplementary material. The CF-A = 1 columns are duplicates of the C1:Berlin row in Figs. 6 and 7. A higher CF-A in Fig. 8 shifts the optimum toward more geothermal capacity and less HT-ATES capacity. Similar discontinuous behavior in optima can be seen as explained in the previous subchapter. A discontinuity of smaller magnitude in LCOH optima for different RES levels (red dots) can be seen at CF-A = 2 and CF-G = 2. In this case, increasing RES to approximately 40% is done by using only geothermal, but beyond this 40% RES, HT-ATES is used. This is due to the sizing effect of the HT-ATES, where very small HT-ATES systems with little heat stored are inefficient [23], leading to a discontinuous behavior of the optimal LCOH at different RES. This figure shows that the optimal sizing is highly dependent on the CF of both technologies, and they essentially compete with each other.

The effect of CF-A when pairing HT-ATES with solar is shown in Fig. 9. The location of the optimum LCOH at different RES (red dots) does not change for the CF-S = 1 and CF-S = 2 rows, indicating that the optimum is completely insensitive to the CF-A as well as the CF-S value. At the CF-S = 0.5 (Fig. 9, third row), with decreasing CF-A value, the LCOH optimum shifts to a larger HT-ATES size, since lower CF-A makes HT-ATES more favorable and therefore more HT-ATES

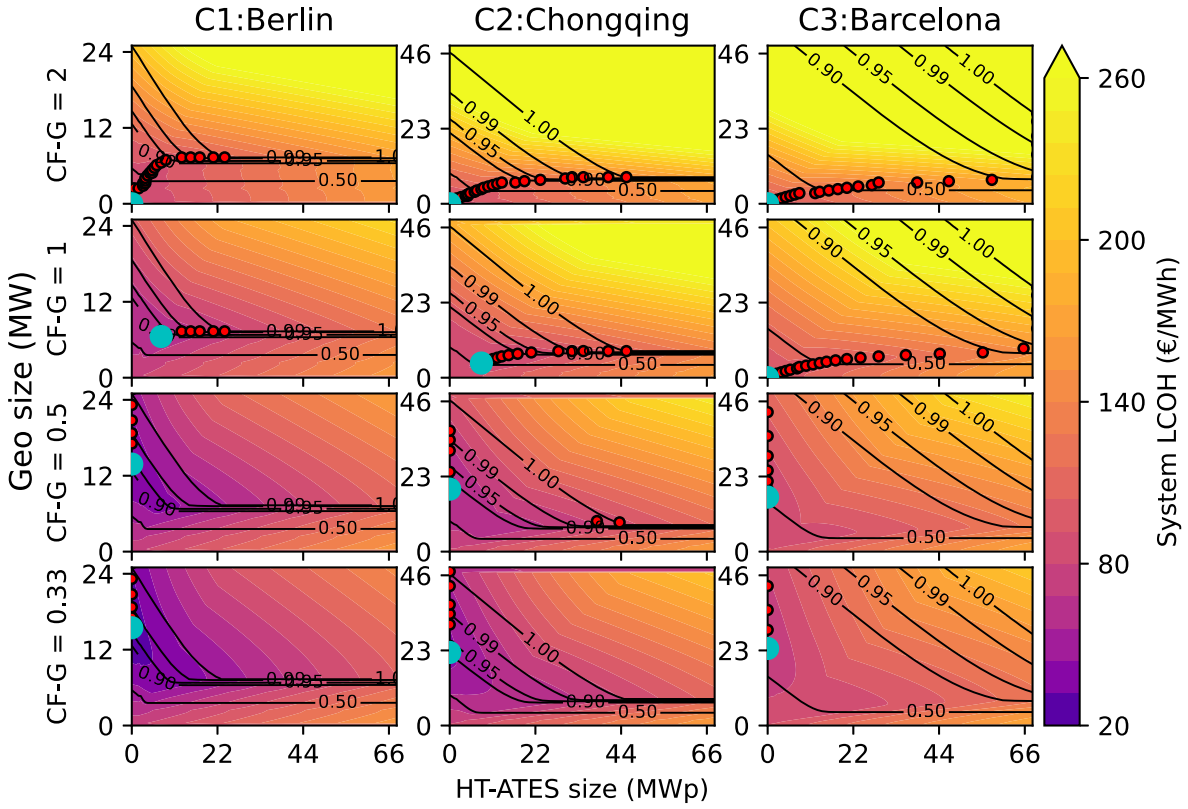

Fig. 6. Influence of the size of Geothermal and HT-ATES on the costs for different clusters and CF-G values. The lines in the plots correspond with the RES. The large cyan dot shows the minimal system LCOH, and the red dots show the minimal LCOH with increasing RES values. Note the different scales on the *x*-axis. The full-sized subplots can be found in the supplementary materials.

capacity is installed. However, also for this CF-S = 0.5 value, the locations of the red dots barely change, indicating again the necessity of installing HT-ATES for reaching larger RES values in these systems and an insensitivity to both the CF-S and the CF-A value.

Comparing the DH with geothermal and with STC, the HT-ATES is shown to be highly cost-effective for the DH system with STC for reaching higher RES targets, while for the DH system with geothermal, the geothermal and HT-ATES are competing with each other. The CF values of both technologies are essential in determining the optimal sizing of the system for the GAG configuration.

Fig. 10 shows which technologies are included in the optimum point (cyan dot in earlier figures) for different CF values. C1:Berlin has the largest potential for geothermal, where a large area of the geothermal plot shows that the optimum consists of something other than only gas. However, the solar plot reveals that the STC should be cheap to be included in the configurations of the optimal point, indicated by the low CF-S values needed for STC to be in the optimum. The STC plots (Fig. 10, bottom row) exhibit a large portion of only gas, which shows that STC is not as cost-effective as geothermal. However, the potential for STC is highest for C3:Barcelona, as their solar resource is larger, due to the city's location. For the 99% RES, the plot is similar (Fig. 11), however, more of the plot includes HT-ATES, compared to the plot discussed earlier, supporting the fact that HT-ATES is efficient at reaching 99% RES. While the optimum with higher CF-A values, did not include HT-ATES, for the 99% RES, it does include HT-ATES.

3.5. Detailed optimum case results

The chosen optima for this part are all using the demand of C1:Berlin, as this cluster represents the most points. For both the GAG and SAG configurations, the chosen points are those with the lowest LCOH (called cost optimum) and those with the lowest LCOH with a RES value of ≥ 99% (called RES99% optimum). For the GAC configuration, these points are selected at an CF-G = 1, while for the SAC configuration, these points are selected at CF-S = 0.5, because at the other CF-S values, the optimum consists of only a gas boiler, providing no further insights. For all optima, the CF-A = 1.

3.5.1. Filled demand profile

The different filled demand profiles can be seen in Fig. 12. Most notable is that for both configurations at 99% RES, the largest peak of demand cannot be covered by renewable sources (Fig. 12(b) and Fig. 12(d)). The solar heat generation is fluctuating, which corresponds to the day and night cycle (Figs. 12(c) and 12(d)). For SAG, the HT-ATES covers a large share of the delivered heat, whereas for the GAG, the geothermal already covers a significant portion of the heat demand.

3.5.2. Minimum LCOH and optimal LCOH at RES99%

A detailed breakdown of the ES and LCOH share of each technology for the chosen optima is shown in Fig. 13. The geothermal delivers more heat directly to the demand compared to the STC. The role of the HT-ATES in achieving 99% RES varies by configuration. In the GAG configuration, when moving from the cost-optimal case to the RES99% optimum, the additional energy is delivered equally between geothermal and HT-ATES. In contrast, in the SAG configuration, the HT-ATES increase in ES is significantly larger than the increase in STC ES. This is due to a mismatch between STC heat generation and heat demand, making the HT-ATES more critical for meeting demand in the SAG configuration. The STC is shown again to be cost-ineffective. For both optima, the LCOH of the SAG configuration is 20% larger than that of the GAG configuration. While the CF-S is 0.5, where CF-G is 1, showing that the STC is significantly more expensive.

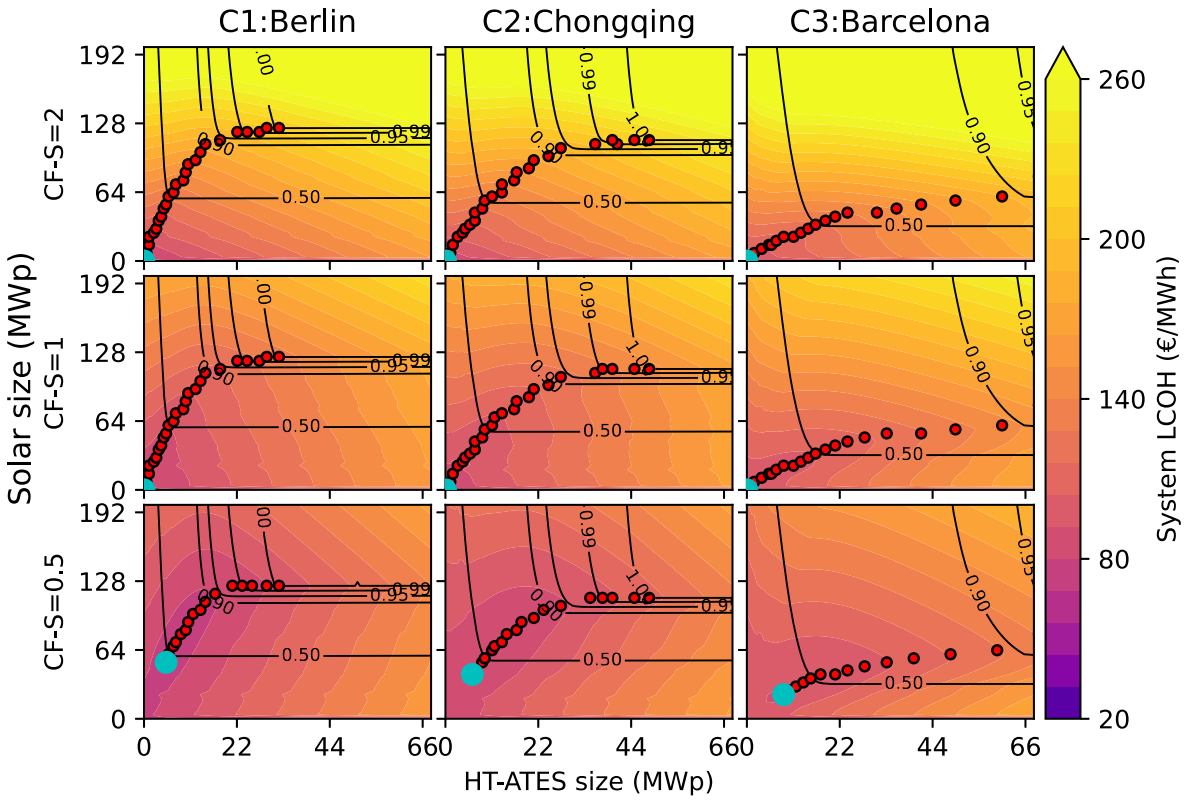

Fig. 7. Influence of the size of STC and HT-ATES on the costs for different clusters and CF-S values. The lines in the plots correspond with the RES. The large cyan dot shows the minimal system LCOH, and the red dots show the minimal LCOH with increasing RES values. The full-sized subplots can be found in the supplementary materials.

3.5.3. Comparison SAG and GAG configuration at RES99%

For both RES99% optima, the gas boiler LCOH is larger than 200 €/MWh, which is due to its relatively large capacity compared to its load. However, only a small share of the energy is provided by the gas boiler, leading to little impact on the system LCOH. For the GAG optima, the geothermal is relatively cheap compared to both HT-ATES and the gas boiler. While for the SAG optima, the HT-ATES is relatively cheap compared to the other technologies due to the high amount of heat stored and delivered by HT-ATES. The STC is more expensive because it delivers less heat directly to the demand, and most of the heat is stored in the HT-ATES, increasing the overall cost.

Lastly, the geothermal is more cost-effective even when CF-G = 1 compared to the solar collector, with CF-S = 0.5. The RES99% optimum of the GAG configuration is comparable in LCOH to the cost optimum of the SAG configuration, which is achieving a RES value of 48%.

3.5.4. Cluster 99% optima comparison

The LCOH and ES for the optimal 99% RES points for the different clusters are shown in Fig. 13. Note here that the actual size of the HT-ATES and geothermal or STC differs between clusters. As seen, the HT-ATES provides comparatively more heat when the peaks are large, seen by the increasing ES of HT-ATES with increasing cluster number. Additionally, the larger peaks also lead to an increased system LCOH, and for C3:Barcelona, the LCOH is very high for both the SAG and GAG configuration compared to the other two clusters, again, due to these high peaks, requiring a large capacity compared to the load. The solar LCOH is decreasing with increasing cluster number, but generally the system LCOH increases.

4. Discussion

In this study, we focused on the optimal sizing of various DH components, using HT-ATES as the selected storage technology. However, other USTES technologies are also relevant alternatives for comparison. Compared to BTES, HT-ATES is expected to cost less for storing the same amount of energy [50], but is less universally applicable, as it requires an aquifer [51]. Welsch et al. [16] observed a similar heat map pattern for the system LCOH when analyzing a system that combines BTES with STC, compared to the SAG configuration [16], showing similar behavior of HT-ATES and BTES. Compared to PTES, HT-ATES is deemed more established [52], where PTES was shown to have higher storage efficiencies [6] but might have land use requirements that are prohibitive in urban settings.

Our results showed that HT-ATES is often used for reaching 100% RES, as it can be more cost-effective to cover the peaks of heat demand compared to increasing STC or geothermal capacity. However, reaching this 100% RES target is very costly, and alternative options should be considered. Examples include demand-side management by the DH operator [53], to reduce the peaks of heat demand as these are the most expensive to cover with renewable technologies. This involves shifting energy consumption from high heat demand periods to times of low heat demand using short-term thermal storage solutions [54]. Another example is to encourage consumers to slightly lower their heat demand by lowering indoor temperatures during peak hours. With appropriate incentives, this behavioral adjustment could contribute to reducing demand peaks [55,56] and reduce the LCOH for achieving 100% RES.

Geothermal is consistently more cost-efficient than STC, while STC competes directly with photovoltaic (PV) solar panels, which also rely on sunlight but convert it to electricity. PV panels are widely deployed due to their competitiveness and short payback period [57,58]. In dense urban areas with limited space, PV adoption will likely be prioritized. In contrast, geothermal for heating purposes faces little direct competition, as using geothermal heat for electricity generation requires exceptionally high temperatures, which are not common in

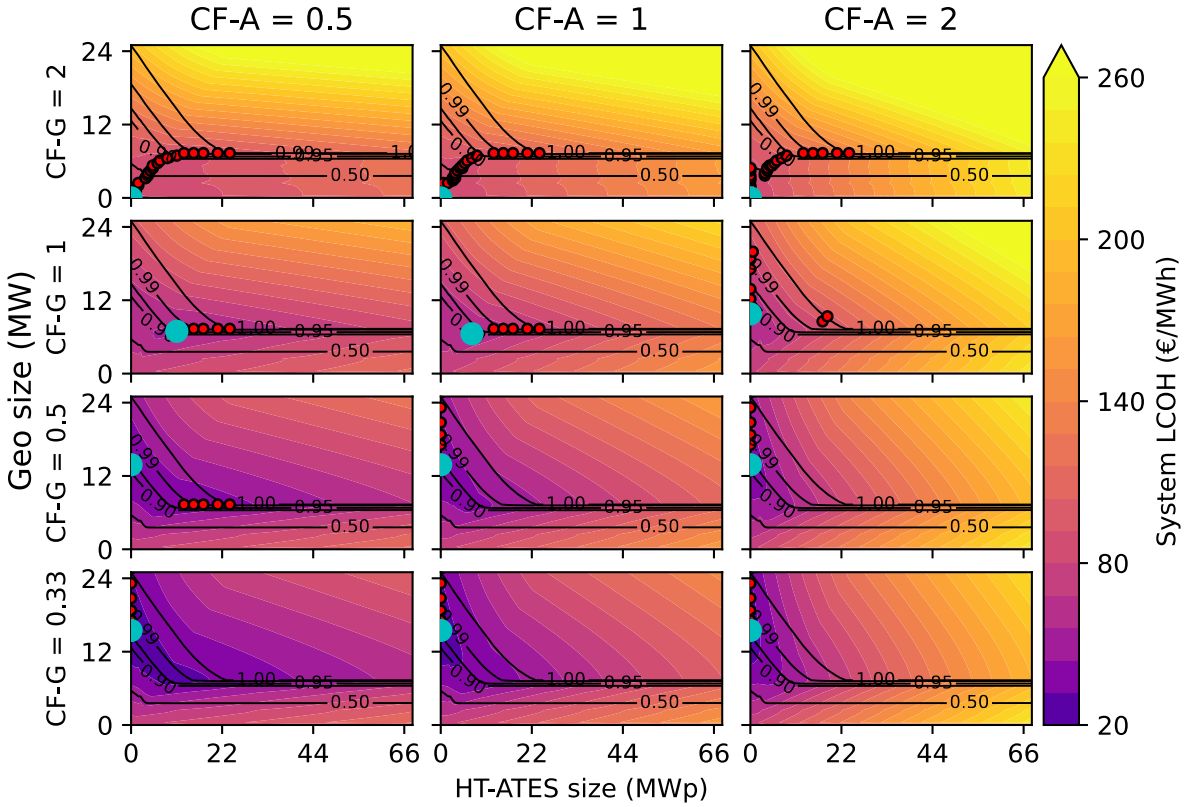

Fig. 8. Influence of the size of geothermal and HT-ATES on the costs for different CF-A and CF-G values. The lines in the plots correspond with the RES. The large cyan dot shows the minimal system LCOH, and the red dots show the minimal LCOH with increasing RES values. This analysis was done for C1:Berlin. The full-sized subplots can be found in the supplementary materials.

urban settings [59]. Furthermore, land required for the geothermal wells is very small, compared to the STC.

Locations with higher geothermal gradients can have a very low CF-G value, below the used CF-G = 0.33 value [60]. The results from EE = 0.33 could be applied here, namely to only use geothermal and no HT-ATES.

Another competing technology is the heat pump, which can be attached to the STC, geothermal, and HT-ATES. They should be considered for case studies and have been shown to be mature [61], with an average coefficient of performance of 3 for high temperature heat pumps (70 °C temperature lift) [62]. However, direct utilization of the heat from DH components was shown to be more cost-effective for HT-ATES [28], as it saves on heat pump investment and operation cost.

4.1. Limitations

The heat demand data used in this study is generated using the method from Staffel et al. [31]. The authors showed that their method contained some errors compared to the actual heat demand, which might affect our results. This method was chosen for its accessibility, but heat demand might not be completely accurate. Additionally, the demand profiles only account for home heating and exclude domestic hot water supply, leading to zero heat demand during summer [63]. The inclusion of domestic hot water demand strongly depends on the specific configuration and responsibility structure of the DH network. In practice, DH systems are not universally responsible for domestic hot water supply. In some cases, DH networks provide only space heating, while domestic hot water is produced locally using electric heaters, heat pumps, or decentralized boilers [64]. Furthermore, even when domestic hot water is supplied by the district heating system, the ratio between space heating demand and DHW demand varies significantly between locations [65].

The heat demand is standardized at 50 GWh across clusters, but due to variations in household energy needs, this amount serves more consumers in C3:Barcelona than in C1:Berlin, possibly requiring a different DH network, affecting network costs [31]. C3:Barcelona already exhibited a generally high LCOH, which will be even larger when the network costs are included.

Another limitation is the assumption of constant yearly heat demand across the system lifetime. In practice, demand is expected to change due to climate change, year-to-year temperature variability, and building retrofits. These changes could influence both optimal component sizing and the resulting LCOH. A structural decrease in annual demand or peak demand—such as through improved insulation—would reduce the required nominal capacity of geothermal, STC, and especially HT-ATES. Because HT-ATES economics are highly sensitive to load factor, lower peaks would make large storage systems less cost-effective and shift the optimum toward smaller storage capacities and lower renewable shares. Conversely, increased demand volatility or extreme winter peaks would require larger geothermal or HT-ATES capacities to maintain high RES levels, increasing CapEx and therefore LCOH. Long-term downward trends in demand also imply that systems optimized for today's demand may become oversized over time, increasing the LCOH due to underutilization of capital-intensive components. Incorporating dynamic demand scenarios could therefore refine the sizing strategy and provide a more realistic range of LCOH outcomes over the system lifetime

From the modeling perspective, there are some limitations, namely, the hydraulics of a DH system are not taken into account. This involves pumps, buffers, and pipe sizing. Additionally, the model assumes perfect heat exchangers, which in practice have an effectiveness up

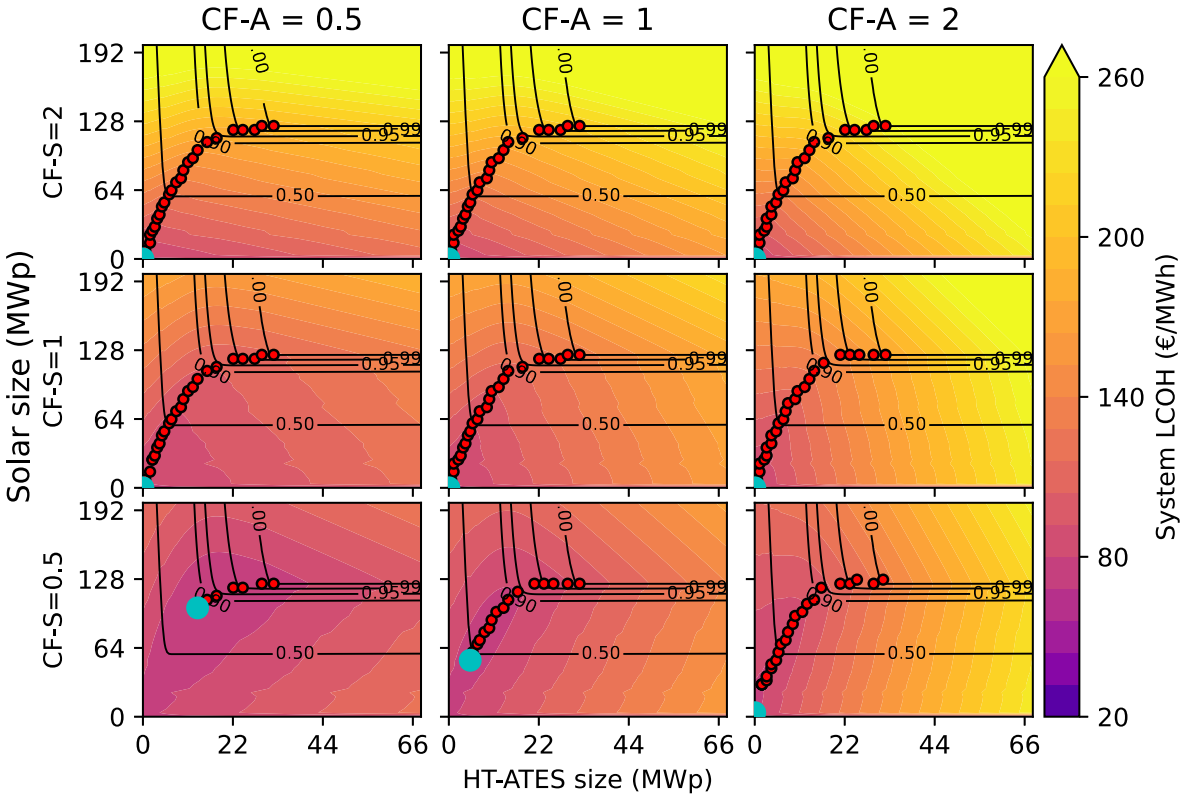

Fig. 9. Influence of the size of STC and HT-ATES on the costs for different CF-A and CF-S values. The lines in the plots correspond with the RES. The large cyan dot shows the minimal system LCOH, and the red dots show the minimal LCOH with increasing RES values. This analysis was done for C1:Berlin. The full-sized subplots can be found in the supplementary materials.

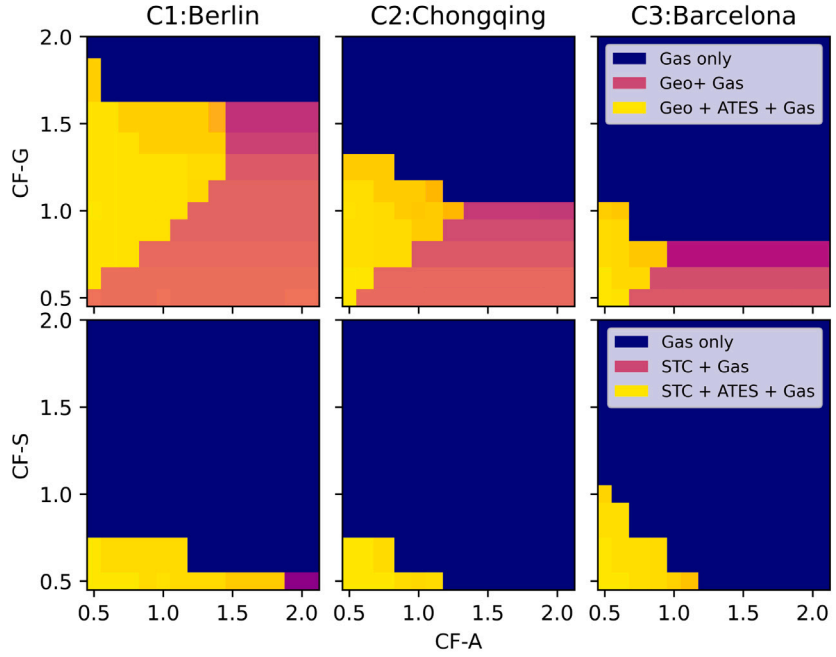

Fig. 10. Effect of the CF-G, CF-S and CF-A on which heat sources are used in the optimum with the lowest LCOH. The top row is with geothermal and the bottom row with STC. The shading in the colors refers to the RES of the optimum, lighter colors indicating a higher RES.

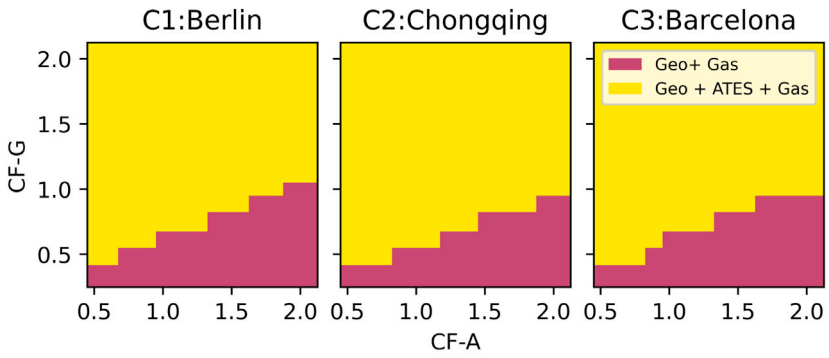

Fig. 11. Effect of the CF-G, and CF-A on heat sources in the 99% RES optimum with the lowest LCOH. STC options are not shown as the whole plot shows STC + ATES + Gas.

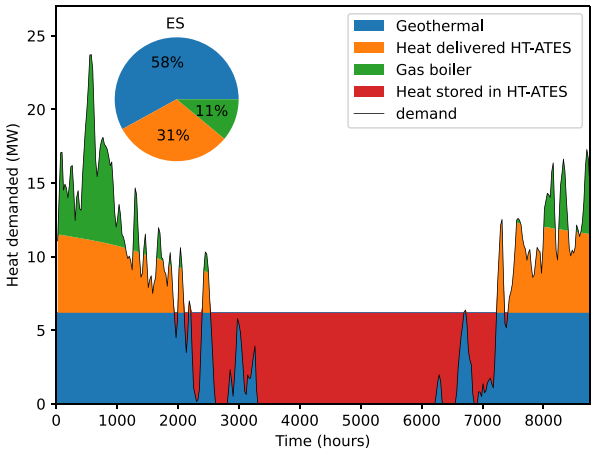

(a) GAG configuration with lowest LCOH. System LCOH = 59€/MWh.

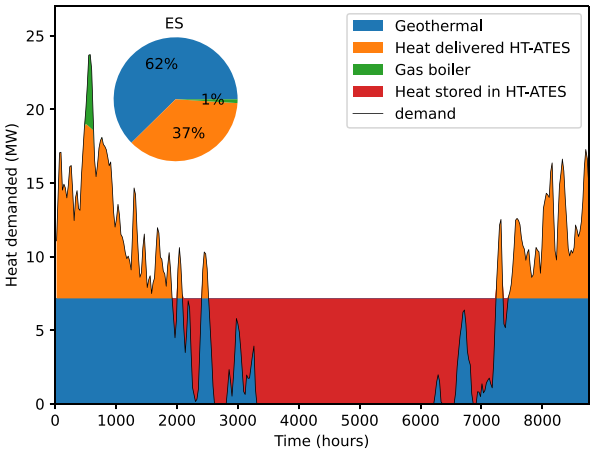

(b) GAG configuration with 99% RES. System LCOH = 66€/MWh.

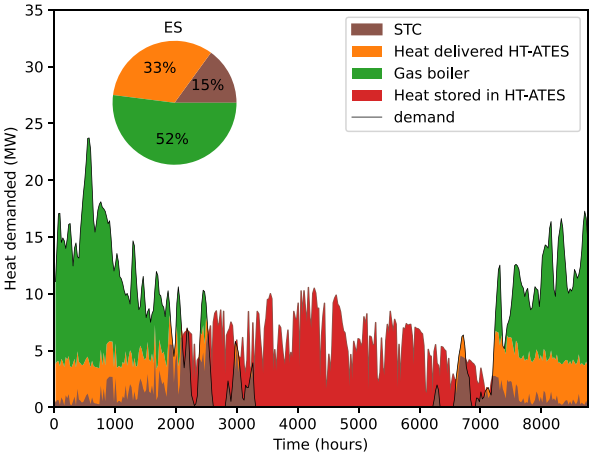

(c) SAG configuration with lowest LCOH. System LCOH = 71€/MWh.

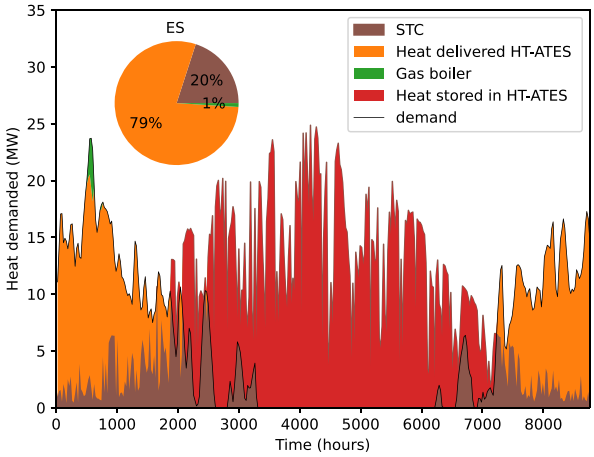

(d) SAG configuration with 99% RES. System LCOH = 81€/MWh.

Fig. 12. Demand profiles of the different chosen optima. The values are averaged over 24 h. The CF-G = 1, CF-S = 0.5 and CF-A = 1. ES is shown in the pie chart.

to 97% [66]. These considerations require detailed simulations at the individual DH level. As this study is focused on heat source sizing across different geographical settings, these details have not been included. Additionally, the costs of installing and operating the DH system were not incorporated into this study. These significantly increase the cost of heat. However, their omission does not affect the determination of the optimal component sizing identified in this study. The optimization performed here is based on relative differences in heat production cost

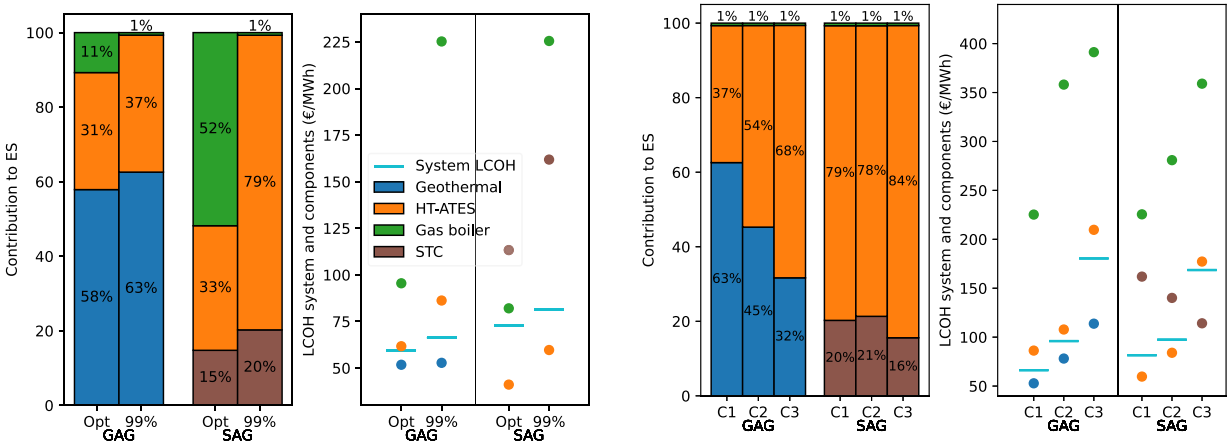

(a) Optimum and RES99% for C1:Berlin

(b) The RES99% of C1:Berlin, C2:Chongqing and C3:Barcelona

Fig. 13. The ES and LCOH of different clusters and chosen optima. The CF-S and CF-A are one. CF-S is 0.5.

under varying generation and storage capacities. Infrastructure-related CapEx and OpEx of the DH network are largely independent of the specific generation mix or component sizing, allowing the omission of the DH network in the cost analysis without weakening the results of this study

From the economic perspective, the study focuses on LCOH, but to have a proper evaluation of the market potential, subsidies should be included. Different countries have different subsidies (for examples, see [67]). These reduce the cost in some way and should be included when doing a more specific study on a DH system. This effect is partly captured with varying EE values, but for case studies, the specific subsidies of that specific city/state should be quantified. However, this falls beyond the scope of the work presented here.

The finding that achieving 100% RES increases the LCOH by approximately 15% relative to 99% RES has important policy and practical implications. It highlights the well-known "last-percentage problem", where the final 1%–10% of decarbonization requires disproportionately large additional capacity that operates at very low load factors. Policymakers aiming for fully renewable district heating systems may therefore need to balance strict RES targets with overall cost-effectiveness, especially in regions where peak-demand coverage drives system cost. Instruments such as targeted capital subsidies, low-interest financing for seasonal storage, or differentiated carbon pricing could help narrow this cost gap by reducing the economic penalty of rarely used capacity. Alternatively, the previously mentioned demand-side management can reduce the peak load that drives the steep cost increase at high RES levels. These measures may enable systems to achieve very high RES targets without requiring excessive oversizing of geothermal or HT-ATES components, thereby mitigating the LCOH increase while preserving progress toward full decarbonization.

5. Conclusion

This study showed the sizing optimization of heat sources and High-Temperature Aquifer Thermal Energy Storage (HT-ATES) to minimize the system LCOH, using different representative demand profiles, different levels of Renewable Energy Share (RES) and further analyzed promising system configurations. The different heat demand profiles were shown to significantly impact the sizing optimization of the District Heating (DH) components and the corresponding Levelized Cost Of Heat (LCOH). The detailed analysis of optimal configurations showed that with larger peak heat demand relative to the average heat demand, more HT-ATES capacity is installed and used to meet these peak loads (seen in the demand profile of C3:Barcelona compared to the demand profile of C1:Berlin). However, these large peaks also lead to a steep increase in LCOH due to a low load factor compared to the capacity of both the renewable source and HT-ATES. For example, the LCOH of the optimum increased by 50% from C1:Berlin to C3:Barcelona.

The optimization results indicate that geothermal is more suitable for supplying heat to a DH system than Solar Thermal Collector (STC), due to its more favorable economic performance and better alignment of its heat output with the heat demand. The LCOH of the SAG configuration is 20% larger than that of the GAG configuration, even if the STC is twice as productive as in its base case. Furthermore, HT-ATES is cost-effective in achieving higher RES values.

With geothermal and HT-ATES, the 90% RES can be reached with less than 5% increase in LCOH compared to the optimal LCOH in most cases. The last few percentages of RES lead to a steep increase in LCOH, as they require a large additional nominal capacity for minimal additional load. In particular, the last 1% of RES leads to a significant increase in LCOH (approximately 15% increase in LCOH compared to 99% RES), highlighting the need to explore alternative solutions for meeting this final increment more cost-effectively.

Based on the research results, the recommendations for the DH planner are to prioritize geothermal where available, use HT-ATES mainly to reach high RES levels without oversizing it. Furthermore, it is important to recognize that 90%–99% RES is far more cost-effective than aiming for 100%. These insights help planners balance cost, system performance, and decarbonization targets

The STC and HT-ATES demonstrated strong synergy, as HT-ATES effectively mitigates the temporal mismatch between STC heat supply and heat demand. In contrast, geothermal and HT-ATES were found to compete in system optimization: when geothermal is sufficiently cost-effective, HT-ATES is excluded from the optimal configuration.

The results of this study provide insights into effective decarbonization strategies for district heating systems and inform the optimal sizing of key system components. The developed code can be applied to other DH systems, with future work exploring different locations and alternative configurations, or assessing specific case studies.

Table A.1
Names of all cities and their corresponding cluster. The bold cities are the cluster centers.

Cluster 1	Cluster 2	Cluster 3
1. Berlin	Chongqing	Barcelona
2. Amsterdam	Ankara	Algiers
3. Astana	Athens	Baghdad
4. Astrakhan	Beijing	Beirut
5. Baku	Chengdu	Houston
6. Calgary	Islamabad	Jacksonville
7. Chicago	Istanbul	Kathmandu
8. Copenhagen	Los Angeles	Lisbon
9. Edinburgh	Phoenix	Nanning
10. Harbin	Rome	Seville
11. Kabul	San Francisco	
12. Kyiv	Shanghai	
13. Lhasa	Tianjin	
14. London	Tokyo	
15. Moscow		
16. New York		
17. Novosibirsk		
18. Osaka		
19. Oslo		
20. Paris		
21. Saint Petersburg		
22. Seattle		
23. Seoul		
24. Stockholm		
25. Tehran		
26. Toronto		
27. Ulaanbaatar		
28. Urumqi		
29. Vancouver		
30. Warsaw		
31. Yekaterinburg		

CRediT authorship contribution statement

David Geerts: Writing – original draft, Visualization, Validation, Software, Methodology, Investigation, Formal analysis, Conceptualization. **Wen Liu:** Writing – review & editing, Supervision, Methodology, Funding acquisition, Conceptualization. **Alexandros Daniilidis:** Writing – review & editing, Supervision, Methodology, Funding acquisition, Conceptualization. **Gert Jan Kramer:** Writing – review & editing, Supervision.

Declaration of competing interest

The authors declare that they have no known competing financial interests or personal relationships that could have appeared to influence the work reported in this paper.

Acknowledgments

This work was funded by the European Union under the Horizon Europe programme (grant no. 1011096566). Views and opinions expressed are, however, those of the author(s) only and do not necessarily reflect those of the European Union or CINEA. Neither the European Union nor CINEA can be held responsible for them.

Appendix A. List of cities for which the demand profiles were obtained and clustering result

In Table A.1, a list of the cities in each cluster can be found.

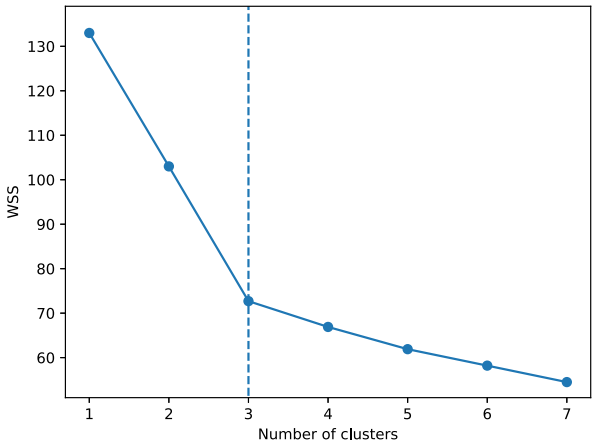

Fig. 14. The elbow curve for the determination of amount of clusters. The elbow point is found at number of clusters of 3.

Appendix B. Robustness of clustering

This section provides more information on the robustness of the clustering. As shown in Fig. 14, the elbow curve shows a dip at n=3, where the Within-Cluster Sum of Squares (WSS) distance does not decrease as significantly as with the addition of the second and third cluster. This supports the statement made in the method. The WSS is based on TimeSeriesKMeans in Python [68].

Data availability

I have shared the link to the github with the data and code.

References

[1] IEA. Space heating. Tech. Rep., IEA; 2023, [Online]. Available: https://www.iea.org/reports/space-heating.
[2] Cozzi L, Gould T, Bouckart S, Crow D, Kim T, Mcglade C, Olejarnik P, Wanner B, Wetzel D. World energy outlook 2020. IEA: Paris, Fr 2020;2050:1–461.
[3] United Nations DoE, Social Affairs PD. World urbanization prospects: The 2018 revision. Tech. Rep., United Nations; 2019, [Online]. Available: https://population.un.org/wup/assets/WUP2018-Report.pdf.
[4] Thiel GP, Stark AK. To decarbonize industry, we must decarbonize heat. Joule 2021;5(3):531–50.
[5] Jodeiri AM, Goldsworthy MJ, Buffa S, Cozzini M. Role of sustainable heat sources in transition towards fourth generation district heating–a review. Renew Sustain Energy Rev 2022;158:112156.
[6] Yang T, Liu W, Kramer GJ, Sun Q. Seasonal thermal energy storage: A techno-economic literature review. Renew Sustain Energy Rev 2021;139:110732.
[7] Bloemendal M, Hartog N. Analysis of the impact of storage conditions on the thermal recovery efficiency of low-temperature ATES systems. Geothermics 2018;71:306–19.
[8] Stemmle R, Blum P, Schüppler S, Fleuchaus P, Limoges M, Bayer P, Menberg K. Environmental impacts of aquifer thermal energy storage (ATES). Renew Sustain Energy Rev 2021;151:111560.
[9] Geerts D, Liu W, Daniilidis A, Vardon PJ, Kramer GJ. Techno-economic analysis of high-temperature aquifer thermal energy storage in district heating systems. Energy Convers Manag: X 2026;101667.
[10] Wang H, Yin W, Abdollahi E, Lahdelma R, Jiao W. Modelling and optimization of CHP based district heating system with renewable energy production and energy storage. Appl Energy 2015;159:401–21.
[11] Morvaj B, Evins R, Carmeliet J. Optimising urban energy systems: Simultaneous system sizing, operation and district heating network layout. Energy 2016;116:619–36.
[12] Liu D-x, Lei H-Y, Li J-S, Dai C-s, Xue R, Liu X. Optimization of a district heating system coupled with a deep open-loop geothermal well and heat pumps. Renew Energy 2024;223:119991.
[13] Friebe M, Karasu A, Kriegel M. Methodology to compare and optimize district heating and decentralized heat supply for energy transformation on a municipality level. Energy 2023;282:128987.

[14] Gabrielli P, Gazzani M, Martelli E, Mazzotti M. Optimal design of multi-energy systems with seasonal storage. Appl Energy 2018;219:408–24.
[15] Chen Y, Guo T, Kainz J, Kriegel M, Gaderer M. Design of a biomass-heating network with an integrated heat pump: A simulation-based multi-objective optimization framework. Appl Energy 2022;326:119922.
[16] Welsch B, Göllner-Völker L, Schulte DO, Bär K, Sass I, Schebek L. Environmental and economic assessment of borehole thermal energy storage in district heating systems. Appl Energy 2018;216:73–90.
[17] Lindenberger D, Bruckner T, Groscurth H-M, Kümmel R. Optimization of solar district heating systems: seasonal storage, heat pumps, and cogeneration. Energy 2000;25(7):591–608.
[18] Raluy RG, Serra LM, Guadalfajara M, Lozano MA. Life cycle assessment of central solar heating plants with seasonal storage. Energy Procedia 2014;48:966–76.
[19] Fiorentini M, Heer P, Baldini L. Design optimization of a district heating and cooling system with a borehole seasonal thermal energy storage. Energy 2023;262:125464.
[20] van der Heijde B, Vandermeulen A, Salenbien R, Helsen L. Integrated optimal design and control of fourth generation district heating networks with thermal energy storage. Energies 2019;12(14):2766.
[21] Dominković DF, Ćosić B, Medić ZB, Duić N. A hybrid optimization model of biomass trigeneration system combined with pit thermal energy storage. Energy Convers Manage 2015;104:90–9.
[22] Sheldon HA, Wilkins A, Green CP. Recovery efficiency in high-temperature aquifer thermal energy storage systems. Geothermics 2021;96:102173.
[23] Geerts D, Daniilidis A, Kramer GJ, Bloemendal M, Liu W. Analytically estimating the efficiency of high temperature aquifer thermal energy storage. Geotherm Energy 2025;13(1):17.
[24] Beernink S, Hartog N, Vardon PJ, Bloemendal M. Heat losses in ATES systems: The impact of processes, storage geometry and temperature. Geothermics 2024;117:102889.
[25] Guglielmetti L, Lehu R, Daniilidis A, Valley B, Moscariello A. Spatial multi-criteria play-based analysis for HT-ATES systems across the Swiss Molasse Plateau. Energy Rep 2025;14:85–102.
[26] Duijff R, Bloemendal M, Bakker M. Interaction effects between aquifer thermal energy storage systems. Groundwater 2023;61(2):173–82.
[27] Beernink S, Bloemendal M, Kleinlugtenbelt R, Hartog N. Maximizing the use of aquifer thermal energy storage systems in urban areas: effects on individual system primary energy use and overall ghg emissions. Appl Energy 2022;311:118587.
[28] Daniilidis A, Mindel JE, De Oliveira Filho F, Guglielmetti L. Techno-economic assessment and operational CO2 emissions of high-temperature aquifer thermal energy storage (HT-ATES) using demand-driven and subsurface-constrained dimensioning. Energy 2022;249:123682.
[29] Bloemendal M, Vardon P, Medema A, Snelleman S, Marif K, Beernink S, van Veldhuizen F, Pijnenborg M, Sudintas G, van Oort T. HT-ATES at the TU delft campus. Tech. Rep.,, TU Delft; 2020, [Online]. Available: https://www.warmingup.info/documenten/window-fase-1—a1—verkenning-hto-tud—feasibilityht_ates_tudelft.pdf.
[30] Heldt S, Beyer C, Bauer S. Uncertainty assessment of thermal recovery and subsurface temperature changes induced by high-temperature aquifer thermal energy storage (HT-ATES): a case study. Geothermics 2024;122:103086.
[31] Staffell I, Pfenninger S, Johnson N. A global model of hourly space heating and cooling demand at multiple spatial scales. Nat Energy 2023;8(12):1328–44.
[32] Geerts D. System-modelling-HT-ATES. 2025, https://github.com/dayfix/System-Modelling-HT-ATES.
[33] Tavenard R, Faouzi J, Vandewiele G, Divo F, Androz G, Holtz C, Payne M, Yurchak R, Rußwurm M, Kolar K, Woods E. Tslearn, a machine learning toolkit for time series data. J Mach Learn Res 2020;21(118):1–6, [Online]. Available: http://jmlr.org/papers/v21/20-091.html.
[34] Geerts D, Daniilidis A, Liu W. A fast and accurate data-driven model for estimating the production temperature of high-temperature aquifer thermal energy storage. Appl Therm Eng 2025;126817.
[35] Gilbert T, Menon AK, Dames C, Prasher R. Heat source and application-dependent levelized cost of decarbonized heat. Joule 2023;7(1):128–49.
[36] Ember. Carbon price tracker. 2024, https://ember-climate.org/data/data-tools/carbon-price-viewer/. [Accessed 25 June 2024].
[37] Lensink S, Eggink E, Schoots K. Eindadvies basisbedragen SDE++ 2024. Tech. Rep., PBL; 2022.
[38] van't Westende J, Dinkelman D. Feasibility study for combined geothermal and HT-ATES systems. Tech. Rep., 2023, [Online]. Available: https://www.warmingup.info/documenten/feasibility-study-for-combined-geothermal-and-ht-ates-systems.pdf.
[39] van de Griendt T. Benefits of high-temperature storage for base load geothermal energy. 2022.
[40] European energy exchange. 2024, https://www.eex.com/en/market-data/natural-gas/indices. [Accessed 25 June 2024].
[41] Wright ML, Lewis AC. Emissions of NO x from blending of hydrogen and natural gas in space heating boilers. Elem Sci Anth 2021;10(1):00114.
[42] Zeilema P. The Netherlands: list of fuels and standard CO2 emission factors version of january 2022. 2022, [Online]. Available: https://www.rvo.nl/sites/default/files/2023-08/The%20Netherlands%20list%20of%20fuels%20and%20standard%20CO2%20emission%20factors%20January%202022.pdf.
[43] Eurostat. Electricity price statistic. 2024, https://ec.europa.eu/eurostat/statistics-explained/index.php?title=Electricity_price_statistics#Electricity_prices_for_non-household_consumers. [Accessed 25 June 2024].
[44] Fleuchaus P. Global application, performance and risk analysis of aquifer thermal energy storage (ATES) (Ph.D. thesis), Karlsruher Institut für Technologie (KIT); 2020.
[45] Greenhouse gas emission intensity of electricity generation in europe. 2025, https://www.eea.europa.eu/en/analysis/indicators/greenhouse-gas-emission-intensity-of-1. [Accessed 07 March 2025].
[46] JRC photovoltaic geographical information system. 2025, https://re.jrc.ec.europa.eu/pvg_tools/en/#MR. [Accessed 06 March 2025].
[47] Bakema G, Drijver B. HEATSTORE state of the art HT-ATES in the netherlands evaluation of thermal performance and design considerations for future projects. 2019, [Online]. Available: https://www.heatstore.eu/documents/HEATSTORE_D1.1_Appendix%20I_final_16-04-2019%20(002).pdf.
[48] Rohde R. Global temperature report for 2024. Tech. Rep.,, California: Berkeley Earth; 2024, [Online]. Available: https://berkeleyearth.org/global-temperature-report-for-2024/.
[49] Commons W. Annual average temperature map. 2014, [Online]. Available: https://commons.wikimedia.org/wiki/File:Annual_Average_Temperature_Map.png.
[50] Lanahan M, Tabares-Velasco PC. Seasonal thermal-energy storage: A critical review on BTES systems, modeling, and system design for higher system efficiency. Energies 2017;10(6):743.
[51] Nordell B, Snijders A, Stiles L. The use of aquifers as thermal energy storage (TES) systems. In: Advances in thermal energy storage systems. Elsevier; 2015, p. 87–115.
[52] Xiang Y, Xie Z, Furbo S, Wang D, Gao M, Fan J. A comprehensive review on pit thermal energy storage: Technical elements, numerical approaches and recent applications. J Energy Storage 2022;55:105716.
[53] Liu H, Du Z, Xue T, Jiang T. Enhancing smart building performance with waste heat recovery: Supply-side management, demand reduction, and peak shaving via advanced control systems. Energy Build 2025;327:115070.
[54] Arnaudo M, Topel M, Puerto P, Widl E, Laumert B. Heat demand peak shaving in urban integrated energy systems by demand side management-a techno-economic and environmental approach. Energy 2019;186:115887.
[55] Csoknyai T, Legardeur J, Abi Akle A, Horváth M. Analysis of energy consumption profiles in residential buildings and impact assessment of a serious game on occupants' behavior. Energy Build 2019;196:1–20.
[56] Cai H, Ziras C, You S, Li R, Honoré K, Bindner HW. Demand side management in urban district heating networks. Appl Energy 2018;230:506–18.
[57] IEA. Renewables 2024. Tech. Rep., Paris: IEA; 2019, [Online]. Available: https://www.iea.org/reports/renewables-2024.
[58] Benli H, Gürtürk M. Investigation of the effect of PV panel efficiency parameter on investment payback period. Int J Innov Eng Appl 2021;5(2):88–92.
[59] IEA. The future of geothermal energy. Tech. Rep., Paris: IEA; 2024, [Online]. Available: https://www.iea.org/reports/the-future-of-geothermal-energy.
[60] Limberger J, Boxem T, Pluymaekers M, Bruhn D, Manzella A, Calcagno P, Beekman F, Cloetingh S, van Wees J-D. Geothermal energy in deep aquifers: A global assessment of the resource base for direct heat utilization. Renew Sustain Energy Rev 2018;82:961–75.
[61] David A, Mathiesen BV, Averfalk H, Werner S, Lund H. Heat roadmap europe: large-scale electric heat pumps in district heating systems. Energies 2017;10(4):578.
[62] Jiang J, Hu B, Wang R, Deng N, Cao F, Wang C-C. A review and perspective on industry high-temperature heat pumps. Renew Sustain Energy Rev 2022;161:112106.
[63] Meha D, Thakur J, Novosel T, Pukšec T, Duić N. A novel spatial–temporal space heating and hot water demand method for expansion analysis of district heating systems. Energy Convers Manage 2021;234:113986.
[64] Zhang L, Xia J, Thorsen JE, Gudmundsson O, Li H, Svendsen S. Technical, economic and environmental investigation of using district heating to prepare domestic hot water in Chinese multi-storey buildings. Energy 2016;116:281–92.
[65] Lidberg T, Olofsson T, Ödlund L. Impact of domestic hot water systems on district heating temperatures. Energies 2019;12(24):4694.
[66] Mahmoudinezhad S, Sadi M, Ghiasirad H, Arabkoohsar A. A comprehensive review on the current technologies and recent developments in high-temperature heat exchangers. Renew Sustain Energy Rev 2023;183:113467.
[67] Interreg North-West Europe. District heating in NorthWest europe. 2024, [Online]. Available: https://vb.nweurope.eu/media/11053/case-to-energy-consumers_web.pdf.
[68] Krzanowski WJ, Lai Y. A criterion for determining the number of groups in a data set using sum-of-squares clustering. Biometrics 1988;23–34.